VII International Conference on Computational Methods for Coupled Problems in Science and Engineering
COUPLED PROBLEMS 2017
M. Papadrakakis, E. Oñate and B. Schrefler (Eds)

DRAG COEFFICIENT OF SPHERICAL PARTICLES IN TURBULENT CHANNEL FLOW

ZDENEK CHARA*, JINDRICH DOLANSKY* AND BOHUS KYSELA*

* Institute of Hydrodynamics CAS, v. v. i.
Pod Patankou 30/5, Prague 166 12, Czech Republic
e-mail: chara@ih.cas.cz, www.ih.cas.cz

Key words: Drag Coefficient, CFD, Lattice Boltzmann Method, Finite Volume Method.

Abstract. *The paper presents results of numerical calculations of drag coefficients of large spherical solid particles. Several hydraulic cases were tested. The first one - the spheres were fixed at different heights above a rough bed of an open channel, the second one - the spheres moved along the channel bed and the third one - the sphere impacted and rebounded from a smooth surface. Finite Volume and Lattice Boltzmann methods were used for the simulations. The Particle Image Velocimetry (2D-PIV) was used to determine the velocity field in the open channel.*

1 INTRODUCTION

The flow of solid particles in a vicinity of a wall is very important for many branches like chemical engineering, civil engineering, environmental problems, hydrotransport. A lot of efforts have been devoted to problems of particles moving in a linear shear flow. The hydrodynamic forces acting on a finite-sized particle moving in a wall-bounded linear shear flow were studied in [1]. The particle Reynolds number varied from 2 to 250. The study showed that the presence of a wall has a significant influence on the drag coefficient. With decreasing a gap size between the particle and the wall the drag coefficient increased. Particle translating and rotating close to a flat wall were studied in [2]. Using DNS simulations a superposition of drag and lift contributions at a modest Reynolds number regime (1-100) was investigated. Measurements of fluctuating forces on a stationary near-bed sediment particle have been performed in [3] for particle Reynolds number range 4000-20000. The results showed that the value of the drag coefficient was about 0.76. Numerical simulations of forces acting on a spherical particle sitting on a bed were performed in [4]. For the calculations the authors used a logarithmic velocity profile as an input. The authors suggested a constant value of the drag coefficient of 0.54 for a range of the Reynolds numbers 1000-10000. They also highlighted an importance of the definition of flow velocity seen by the particle for the calculation of the drag coefficient.

The main objectives of this study are to numerically simulate a flow around large spherical particles in a water channel flow. The ratios of flow depth to particle diameters are 2.5 and 6.8 respectively. In this study we have focused on an initial stage of the particle movement up to $t^* = t\,u/D = 40$.

2 GEOMETRICAL ARRANGEMENT

Schematic view of the geometrical arrangement for the numerical simulations is shown in Fig. 1. The bottom of the channel was covered by a one layer of glass rods of diameter 6 mm. The rods were placed perpendicularly on the flow direction. The spheres of diameters D were fixed in different heights, h, above the bottom. Two smooth spheres of diameter 25.4 and 10 mm were used. The channel flow depth was 65 mm (measured form the center of the bed rods) and the mean velocity was 0.5 m/s. The bulk Reynolds number calculated form the mean velocity and the flow depth was Re = 31000. The gaps between the sphere and the bottom were h=2; 4.3 and 10 mm for the larger particle (D=25.4 mm) and h= 4.3 and 10 mm for the second sphere (D=10 mm). We also tested an influence of the particle rotation on the drag coefficient so the larger sphere placed 4.3 mm above the bottom was allowed to free rotate with an angular velocity ω=60 rad/s at the clock-wise direction about the transverse axis (the flow direction is from the left to the right, see Fig. 1).

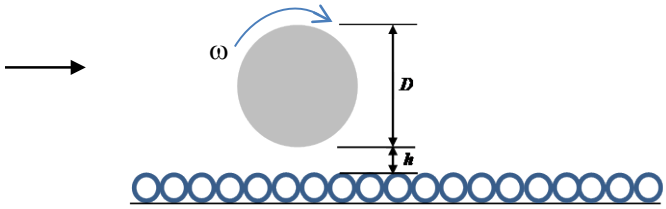

Figure 1: Schematic view

Similar hydraulic conditions were used for the experimental part. The experiments were performed in the horizontal open channel of a cross section 0.25x0.25 m and length 6 m. Both the side walls and the bottom are made from glass plates. As for the numerical simulations the channel bottom was covered by one layer of the glass rods of diameter 6 mm. The rods were placed perpendicularly on the flow direction. The 2D PIV system consisted of a camera NanoSense MK III with 4 GB inner memory and frame rate 1000 fps in full resolution 1280x1024 pixels. The capacity of the camera inner memory enabled to pick up the frames in a total time 3.3 sec. The seeding particles used were hollow glass 10 μm particles (Dantec Inc. DK). As the sources of illumination were used Leica KL2500LCD equipped with lightline with adjustable focusing optics. This light source worked in a continuous mode. The lights were placed above the water level and under the channel bottom. The flow depth in the measuring section was H=64 mm and the flow rate was 8.6 l/s. The bulk flow Reynolds number was Re=33000.

3 NUMERICAL SIMULATIONS

The CFD conducted in this study were large eddy simulations - LES implemented in FVM (Ansys Fluent) and LES implemented in a in-house code of LBM. Size of a computational domain for the channel flow simulated by the FVM was 4.6H x H x 2H where H is the open channel flow depth. Smagorinksy-Lilly approach was used as the sub grid model with C_s=0.14. To achieve a reasonable turbulence level a simulation without the spherical particles was performed. We used periodic flow conditions at the inlet and outlet boundaries and on the side walls a symmetry condition was applied. The water flow surface was modelled as a wall

with zero shear stress. A thickness of the first layer of the boundary layer on the particle surface was 0.05 mm and time steps of the calculations were 0.0005-0.001 sec. The computational mesh consisted of 8.6 million mostly tetrahedron cells.

The channel flow was also modelled using the lattice Boltzmann (LBM) based simulation. The LBM represents a recent numerical approach which excels thanks to its effectiveness and straightforwardness in modeling arbitrary boundaries. The lattice Boltzmann equation

$$f_i\left(\mathbf{x}+\mathbf{c}_i\Delta t, t+\Delta t\right)-f_i\left(\mathbf{x},t\right)=\frac{1}{\tau}\left(f_i^{eq}-f_i\right) \tag{1}$$

represents a discrete analogy to the continuous Boltzmann equation and it is derived by discretization in time and space, and by choice of the discrete velocity space (meaning of individual symbols follows in the text). The LBE describes dynamics of fictive particles propagating along links of an orthogonal lattice, given by the choice of discrete velocities $\mathbf{c}_i$, and interacting in the nodes of the lattice. The fictive particles are represented by distribution functions f_i which give probabilities of finding a fictive particle in a certain time t in a certain node $\mathbf{x}$ with a certain discrete velocity $\mathbf{c}_i$. The LBE can be evaluated in two steps: the stream or propagation step which is described by the left hand side of the LBE, and the collision step which is determined by the term on the right hand side of the LBE. In the first step the values of the distribution functions are shifted to the neighboring nodes along the corresponding directions. In the second step the fictive particles interact in the nodes which is realized through relaxation to the equilibrium distribution functions f_i^{eq} and the rate of the relaxation is given by the relaxation time τ. The total interaction which includes the relaxation is determined by the collision operator. In the examined simulation the LBGK operator, which conserves mass and momentum, with single relaxation time τ was used. From locality of both steps follows possible parallelization of the LBM which leads to its mentioned effectivity.

As the considered flow is characterized by high values of the Reynolds number, the LBM based simulation was enriched by a Smagorinsky subgrid model which modified the value of the relaxation parameter in each node to model influence of unresolved scales on the flow. On the surface of the moving sphere the no-slip boundary condition is imposed which is implemented by the bounce-back algorithm where contribution of momentum transfer from the moving sphere is included. The force, which the flow exerts on the sphere as it moves through the channel, is given by the sum of contributions of incoming and outgoing fictive particles over all boundary nodes

$$\mathbf{F}=-2\sum_{\mathbf{x}_b}\sum_{i}\left(f_i-\frac{w_i}{c_s^2}\rho\left(\mathbf{c}_i\,\mathbf{v}\right)\right)\mathbf{c}_i \tag{2}$$

where w_i represents weights for different lattice directions, c_s is the lattice sound speed, ρ is the flow density and v is the velocity of the sphere. Three different lattice boundary schemes are employed to model boundaries of the channel. The side walls, the inflow and the outflow are connected by the periodical condition, the bed surface is simulated by the bounce-back algorithm and the free surface of the flow is implemented with the help of the modified symmetric condition.

The in-house simulation employed the standard D3Q19 lattice to study the examined process. The computational domain made of 400 × 91 × 91 nodes corresponded to 0.3 × 0.068 × 0.068 m which led to the space step $\Delta x = 7.5 \times 10^{-4}$ m. This resolution determined the number of 34 nodes per the particle diameter D=25.4 mm. Although there is no

straightforward way to choose Δt with respect to Δx within the LBM it was assumed that the order of the time step and the space step were related as $\Delta t / \Delta x = 0.1$.

4 RESULTS AND DISCUSSION

The initial stage of the numerical simulations was focused on the flow around the sphere placed at a stream of a constant velocity without any wall effect. The FVM approach was used. A computational domain of dimensions 0.25 x 0.1 x 0.1 m was built and inside the box we placed the sphere of the diameter D=25.4 mm. The input velocities were 0.15 and 0.47 m/s (Re=3800 and 12000). We also studied a combination of input velocities and streamwise rotation of the angular velocity ω=60 rad/s. The flow was impulsively started from zero to given velocity. The vortex structures behind the sphere are shown in Fig. 2 for the input velocity 0.15 m/s and in Fig. 3 for the input velocity 0.47 m/s. The flow direction is from the left to the right. The vortices are visualized as isosurfaces of the Q-criterion (Q=10 s^{-2}). A relatively stable primary vortex can be seen in the plots (a) and (c) which show the situation without particle rotation for different non-dimensional times $t^* = t\, u/ D$. Due to the rotation the vortical structures are deformed even for low values of the non-dimensional time. Values of the longitudinal force (F) were recorded and finally the drag coefficient was calculated from well-known equation $C_d=F/(0.125\rho u^2 \pi D^2)$. The results are shown in Fig. 4 for the both Reynolds numbers. The drag coefficient of non-rotating sphere of Re=3800 is about C_D=0.43 which corresponds to literature data. For the rotating sphere the drag coefficient significantly fluctuates and its mean value is about C_D=0.51. For Re=12000 the drag coefficient of the non-rotating sphere more or less corresponds to values of lower Re up to t^*=20. In a range $20<t^*<30$ a remarkable increase of the drag coefficient can be observed. In that region the flow behind the sphere becomes fully turbulent. For a region $t^*>30$ the values of the drag coefficient smoothly approach the data of the lower Re. For rotating sphere of Re=12000 the transition to turbulence occurs sooner (t^*=6) and the values of the drag coefficient are higher C_D=0.61.

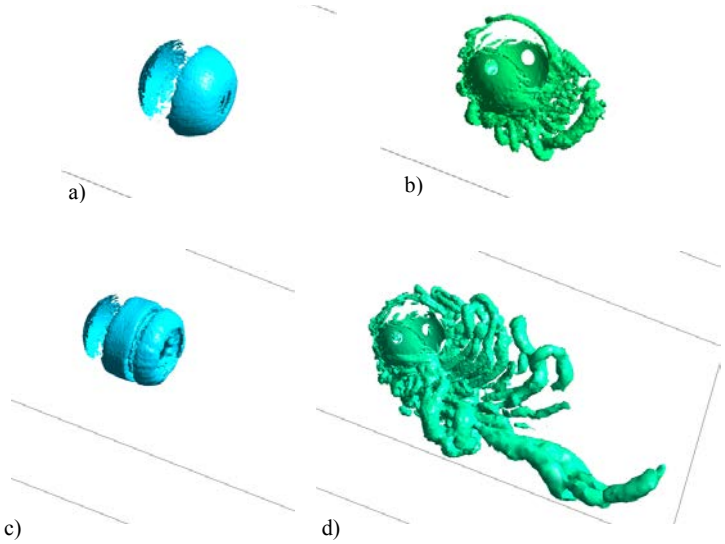

Figure 2: Isosurfaces of the Q-criterion (Q=10 s^{-2}) - a) u=0.15m/s, ω=0, t^*=1.8; b) u=0.15m/s, ω=60, t^*=1.8; c) u=0.15m/s, ω=0, t^*=5.9; d) u=0.15m/s, ω=60, t^*=5.9

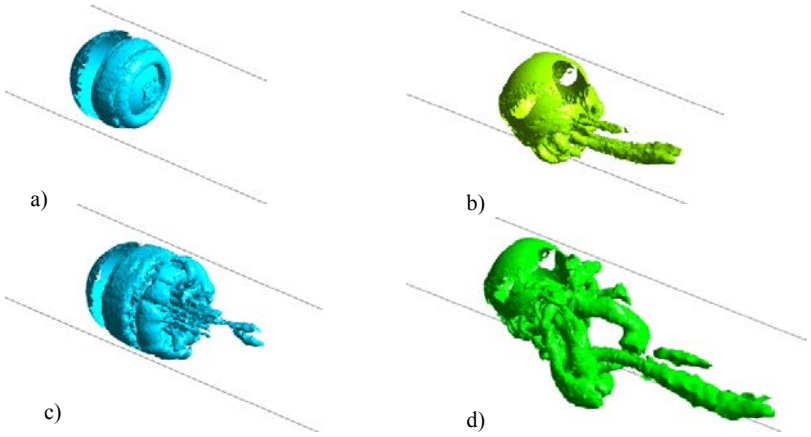

Figure 3: Isosurfaces of the Q-criterion (Q=10 s^{-2}) - a) u=0.47m/s, ω=0, t*=3.7; b) u=0.47m/s, ω=60, t*=3.7; c) u=0.47m/s, ω=0, t*=7.4; d) u=0.47m/s, ω=60, t*=7.4

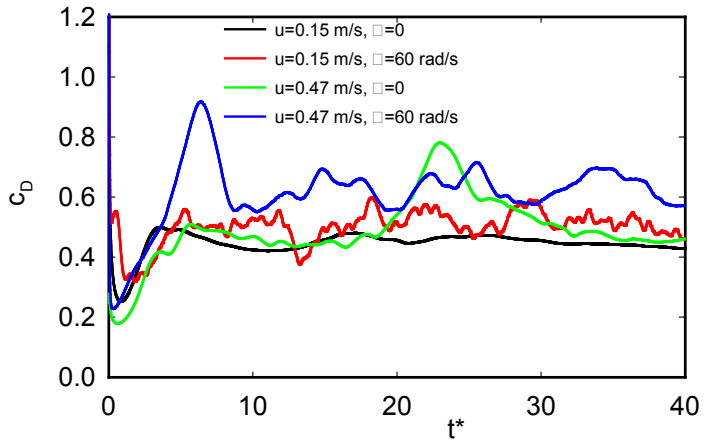

Figure 4: Time histories of the drag coefficients (D=25.4 mm) – constant velocity input

We also simulated an impact of the sphere with smooth wall in the normal direction and a rebound of the sphere from the wall. We used the same computational domain as in the previous case. To avoid difficulties of a grid remeshing close to the sphere surface the sphere was fixed at the initial position above the wall (L/D=4.7) and whole computational box was allowed to move with a constant velocity 0.15 m/s (Re=3800). When the sphere came near the wall the motion was stopped and after a short time (4 ms) the box moved at opposite direction with the same velocity (0.15 m/s). The force on the sphere surface was recorded and the drag coefficient was subsequently calculated. The results are shown in Fig. 5 where t*=0 corresponds to a time of the impact. When the gap between the sphere and the wall is about one sphere diameter the drag coefficient increases up to a value C_D =1.3. But in our case the sphere did not touch the wall (the final gap was 1.5 mm) and the drag coefficient will be probably higher just at the impact. The rebounding phase is characterized by a fluctuation of the drag coefficient.

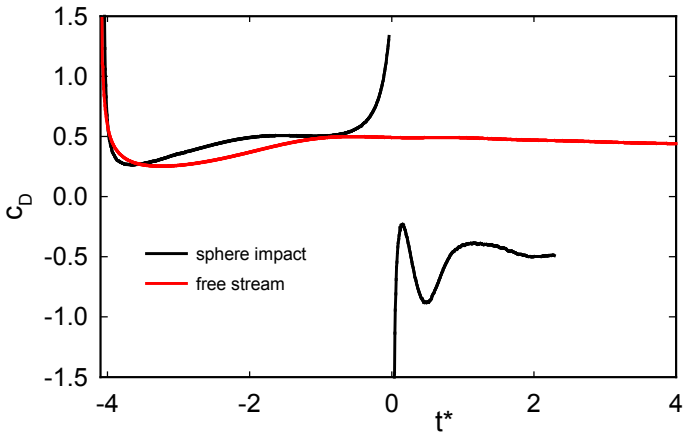

Figure 5: Time history of the drag coefficient during the normal impact with the wall (D=25.4 mm)

The FVM simulation of the channel flow consisted of two steps. The first step was a simulation of the channel flow without any particles. During this phase turbulent flow conditions were achieved. At the second phase the resulted data of velocities and pressure were interpolated onto the computational domain with the particle and the simulation was initialized. It means that the flow around the sphere impulsively started from the time of the initialization. In the case of the LBM-LES simulation a power law equation was used to initialize the velocity profile inside the domain. A comparison of the simulated and measured non-dimensional velocity profiles is shown in Fig. 6. The particle Reynolds numbers were calculated from the mean velocities at positions corresponding to the centers of the particles. The particle Reynolds numbers varied from 4000 (D=10 mm) to 12000 (D=25.4mm).

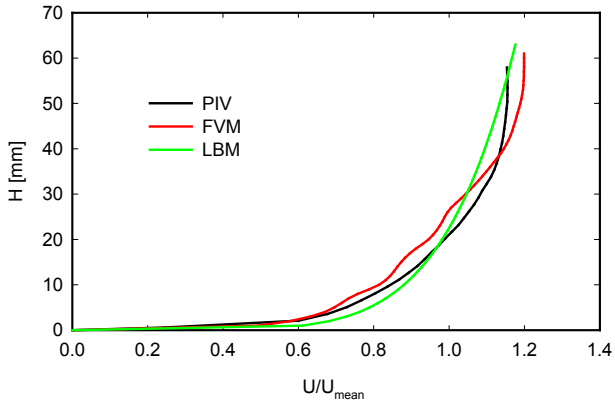

Figure 6: Profiles of the channel mean velocities

The spherical particles were fixed at different positions above the rough bed. For the gap height h=4.3 mm and the particle diameter D= 25.4 mm isosurfaces of the vortex Q parameter are shown in Figs. 7, 8 and 9. Fig. 7 shows the results of the FVM simulations for the non-rotating sphere at different non-dimensional times. Due to the higher velocity at the top of the sphere the primary vortex ring is deformed and it is transported to the central part of the main flow. On the contrary due to the particle rotation (at clockwise direction) the primary

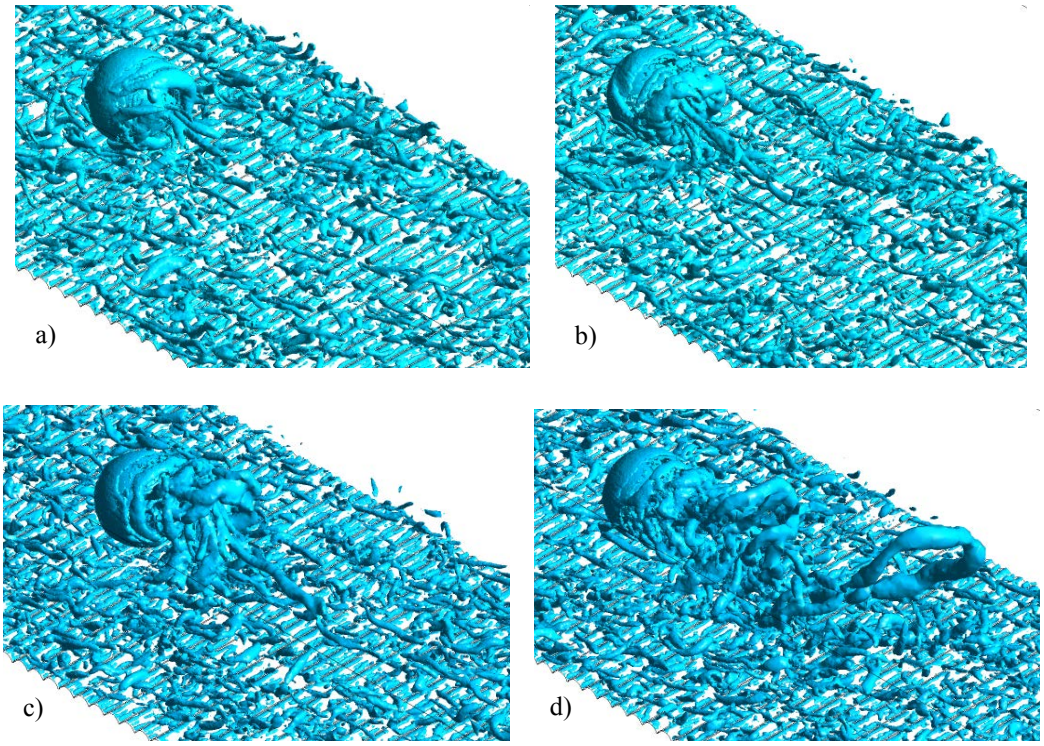

Figure 7: Isosurfaces of the Q-criterion (D=25.4 mm, h=4.3 mm) – a) t^*=1.5, b) t^*=2.2, c) t^*=3.6, d) t^*=7.2

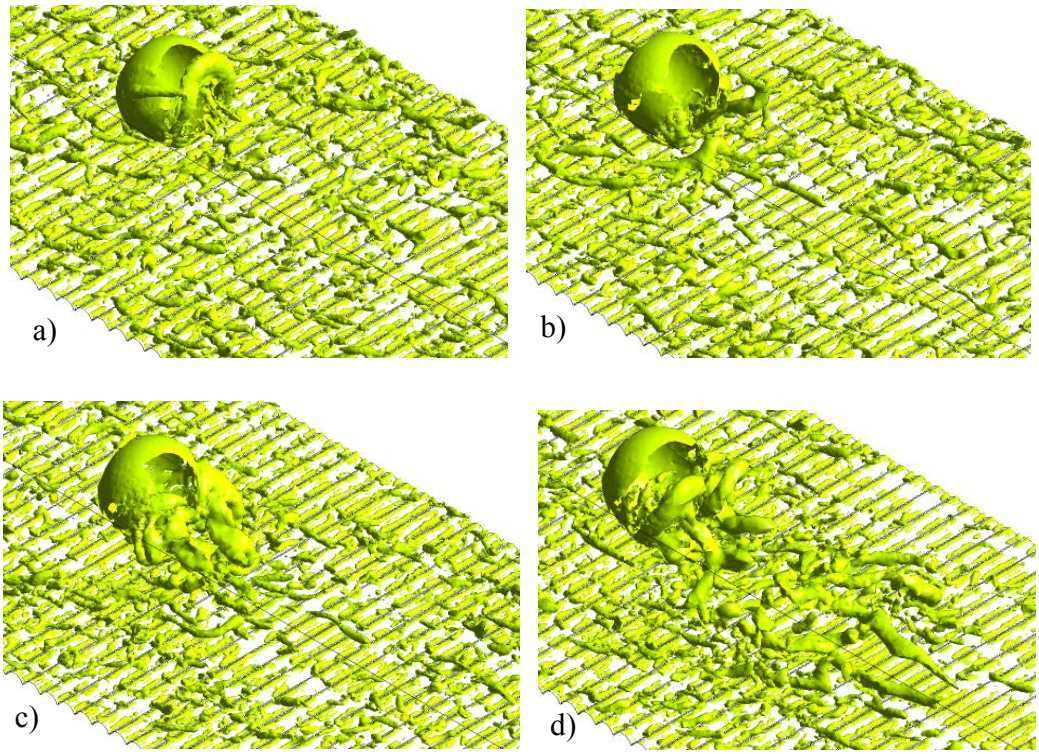

Figure 8: Isosurfaces of the Q-criterion (D=25.4 mm, h=4.3 mm, ω=60 rad/s) – a) t^*=1.5, b) t^*=2.2, c) t^*=3.6, d) t^*=7.2

vortex is not developed, see Fig. 8. Fig. 9 shows the results of the LBM-LES simulations for the non-rotating particle at the same position (h=4.3 mm). The LBM-LES simulation seems to break the main vortical structure into small vortices during a shorter time.

The resulting time histories of the drag coefficients for the larger sphere (D=25.4 mm) are plotted in Fig. 10. For the gap height h = 10 mm the values of the drag coefficients correspond to the values calculated for the free stream input. With decreasing heights of the gap the drag coefficients are increasing. For the gap height h=4.3 mm the value of the drag coefficient is about 0.58, for h = 2 mm the drag coefficient is about 0.63 and for h = 4.3 mm and rotation of ω = 60 rad/s the drag coefficient is about 0.70. The results of the both simulations are in a good agreement. The history of the drag coefficient development for smaller particle (D =10 mm) is shown in Fig. 11. No significant influence of the gap height on the drag coefficient was observed. The drag coefficient in the channel flow is about 10 percent higher compare to the free stream.

The LBM-LES was used to simulate the motion of the spherical particle parallel to the channel bottom. The larger particle (D = 25.4 mm) was initially placed at a position 10 mm above the bottom. The particle moved along the bottom by a constant velocity 0.45 m/s. The channel point velocities were modelled by the power law equation. The developed vortical structures are shown in Fig. 12 as isosurfaces of the Q-criterion. The vortices are relatively stable compare to the flow around fixed particle.

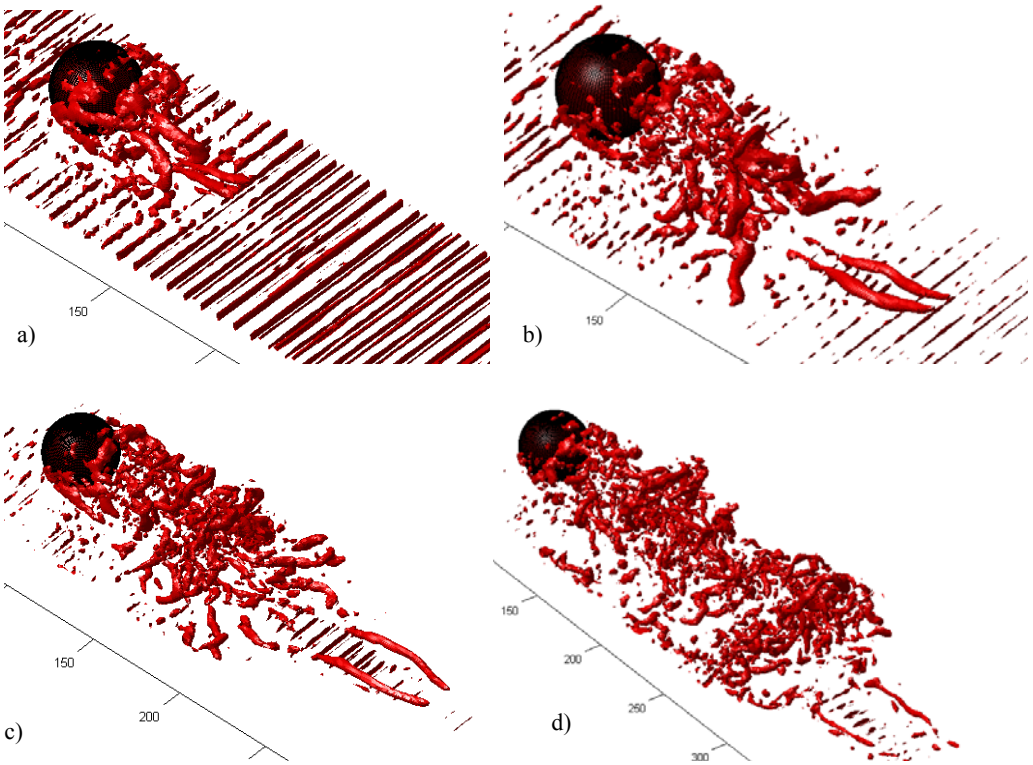

Figure 9: Isosurfaces of the Q-criterion (D=25.4 mm, h=4.3 mm, LBM-LES) – a) t^*=1.8, b) t^*=3.6, c) t^*=5.4, d) t^*=9.1

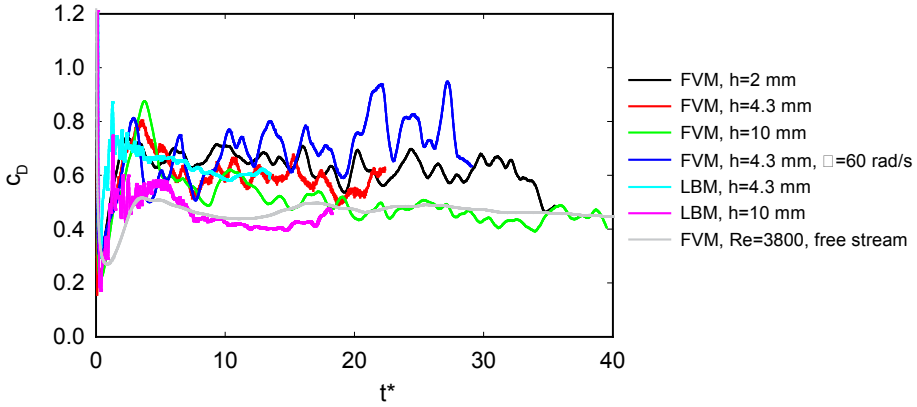

Figure 10: Time histories of the drag coefficients (D=25.4 mm) – channel flow

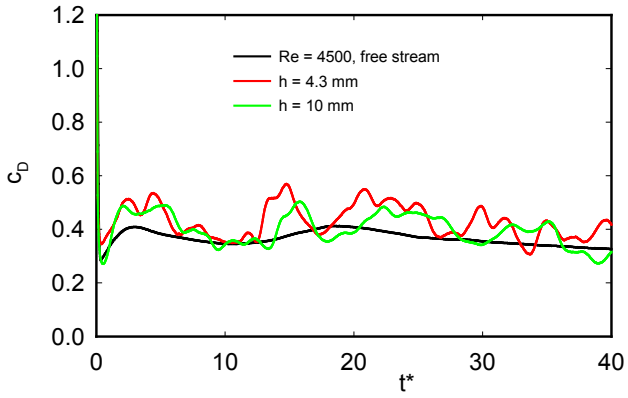

Figure 11: Time histories of the drag coefficients (D=10 mm) – channel flow

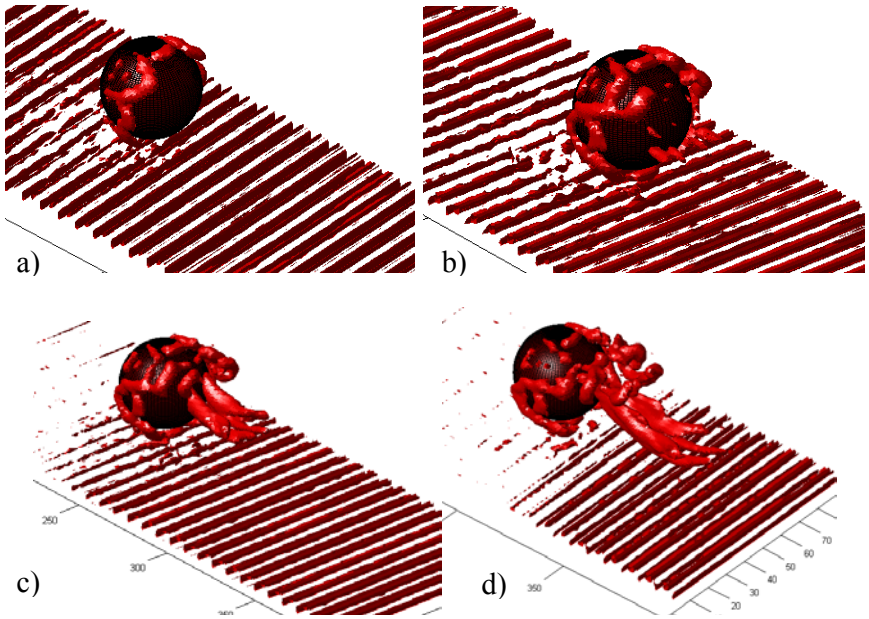

Figure 12: Isosurfaces of the Q-criterion - moving sphere (D=25.4 mm, h=10 mm, LBM-LES) – a) t*=1.8, b) t*=3.6, c) t*=5.4, d) t*=7.1

5 CONCLUSIONS

The paper presents numerical simulations of the flow around large spherical particles. Several geometrical arrangements were studied. The particles were flowed around by a free stream input, the particle impacted and rebounded from a wall, the particles were fixed at different position above rough bed in the channel flow and the particle moved parallelly along the bed. The forces acting on the particle were monitored and the drag coefficients were calculated. It was shown that the drag coefficient is increasing with decreasing the gap height between the particle and the bed.

ACKNOWLEDGEMENT

The supports under project No. 15-18870S of the Grant Agency of the Czech Republic and RVO: 67985874 are gratefully acknowledged.

REFERENCES

[1] Zeng, L., Najjar, F., Balachandar, S. and Fischer,P. Forces on a finite-sized particle located close to a wall in a linear shear flow. *Phys. Fluids* (2006) **21**, 033302.

[2] Lee, H. and Balachandar S. Drag and lift forces on a spherical particle moving on a wall in a shear flow at finite Re. *J. Fluid Mech*. (2010), **657**, 89–125.

[3] Schmeeckle, M. W., Nelson, J.M. and Shreve R.L. Forces on stationary particles in near-bed turbulent flows, *J. Geophys. Res*. (2007) **112**, F02003.

[4] Lee, H. and Balachandar S. (2012), Critical shear stress for incipient motion of a particle on a rough bed, *J. Geophys. Res*., (2012) **117**, F01026.